

# Chemical Bonding and Band alignment at $X_2O_3/GaN$ ( $X=Al,Sc$ ) interfaces

Zhaofu Zhang,<sup>1</sup> Yuzheng Guo,<sup>2</sup> and John Robertson<sup>1, a)</sup>

<sup>1</sup>*Department of Engineering, Cambridge University, Cambridge, CB2 1PZ, United Kingdom*

<sup>2</sup>*College of Engineering, Swansea University, Swansea, SA1 8EN, United Kingdom*

*a) E-mail address of corresponding author: jr214@cam.ac.uk*

The chemical bonding and band alignment at  $Al_2O_3/GaN$  and  $Sc_2O_3/GaN$  interface are studied using density functional supercell calculations. Using bonding models based on the electron counting rule, we have created the insulating interfaces with small roughness and a clean bandgap. Ga-O bonds dominate the interfacial chemical bonding for both interfaces. The calculated band alignment agrees with the experimental values. For the  $Al_2O_3$  interface, the calculated valence band offset is 1.17 eV using hybrid functionals, while that for the  $Sc_2O_3$  interface is 0.81 eV. The conduction band offsets are both larger than 1 eV, and as large as  $\sim 2$  eV for the  $Al_2O_3$  interface. The calculated band alignments indicate that  $Al_2O_3$  and  $Sc_2O_3$  are both suitable insulators for GaN-based MOSFET applications.

Wide bandgap semiconductor GaN-based metal-oxide-semiconductor field effect transistors (MOSFETs) are promising candidates for next-generation high-voltage power devices beyond silicon.<sup>1,2</sup> Nevertheless, large concentrations of surface and/or interface states has hindered the device performance, leading to leakage currents and current collapse.<sup>3</sup> To maximumly supplement the flexibility of device design and enable novel functionalities in GaN-based electronics, the gate dielectric should be prudently selected.  $Sc_2O_3$  with large bandgap ( $\sim 6$  eV), high dielectric constant ( $\epsilon=14$ ), and large band offset (BO) has been reported to deliver low density of interface states ( $D_{it}$ ) of  $\sim 10^{12}$  eV<sup>-1</sup>cm<sup>-2</sup> with little leakage current at the  $Sc_2O_3/GaN$  interface in the past decade.<sup>4,5</sup> Later, the industrially preferred oxide  $Al_2O_3$  became popular by virtue of high breakdown electric field ( $\sim 10$  MV/cm), high thermal stability, favorable band alignment with GaN, as well as an easier preparation by atomic-layer deposition (ALD) technique,<sup>6-9</sup> and the device performance has been dramatically improved.<sup>10,11</sup> Thus, both  $Sc_2O_3$  and  $Al_2O_3$  are suitable insulator materials for GaN-based MOSFET devices.

The interfaces of both oxide dielectrics on GaN have been extensively studied experimentally. The band offset especially the conduction band offset (CBO) should be sufficiently large ( $> 1$  eV) to inhibit Schottky emission of carriers and suppress the leakage current for a high-quality oxide/GaN interface.<sup>12,13</sup> In power devices, a larger CBO is more desirable considering the high-voltage gate driver requirement. Some previous work has reported the experimental BO values between GaN and oxide by x-ray photoemission spectroscopy (XPS), while the reported valence band offsets (VBO) have a wide range of values from 0.05 eV to 2.1 eV for  $Al_2O_3$  interface,<sup>6-9,14</sup> and 0.4-0.8 eV for the  $Sc_2O_3$  interface.<sup>15,16</sup> The large uncertainty brings trouble for fully understanding the quality of gate oxide. Furthermore, the microscopic understanding of the oxide/GaN interface properties is hindered by a lack of theoretical work on the detailed chemical bonding and band alignment of reasonable  $Al_2O_3/GaN$  and  $Sc_2O_3/GaN$  configurations. The accurate BOs should be attained based on the stable and insulating interface, where there are no gap states within the bandgap and the Fermi level lies at midgap. To achieve this goal, the electron counting rule (ECR) must always be obeyed while constructing the interface.<sup>17-19</sup> Currently, there are only two calculations of the  $Al_2O_3/GaN$  interfaces, but these used the  $\alpha$ - $Al_2O_3$  phase which has too large a band gap ( $\sim 8.8$  eV), and the importance of electron-counting was ignored.<sup>20,21</sup>

In this work, the geometry and electronic properties of the interface between GaN and two trivalent oxides  $X_2O_3$  ( $X=Al, Sc$ ) are investigated in detail by first-principles calculations. To derive the band line-up with GaN, we first constructed  $X_2O_3$ /GaN interface models for a less ionic oxide  $Al_2O_3$  and a more ionic oxide  $Sc_2O_3$ . The band offsets are then derived using the core-level method in the insulating interfaces.<sup>22</sup> Our results validate a VBO of 1.17 eV and 0.8 eV for  $Al_2O_3$ /GaN and  $Sc_2O_3$ /GaN, respectively, both within the range of measured values.

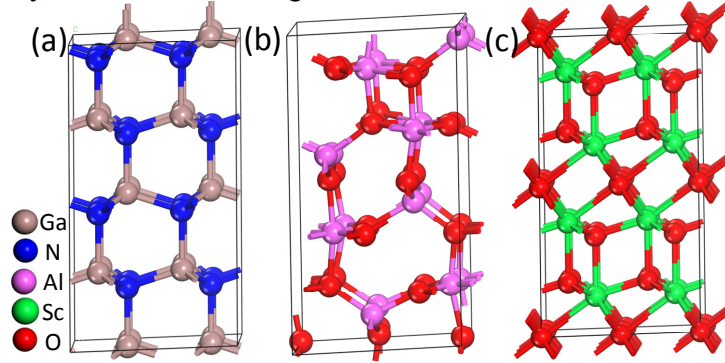


FIG. 1. The final relaxed structures of (a) GaN, (b)  $Al_2O_3$  and (c)  $Sc_2O_3$  bulk, respectively. The species of atoms are indicated in the insert.

The calculations were carried out using the density functional theory (DFT) plane-wave CASTEP code.<sup>23,24</sup> Norm-conserving pseudopotential with a plane-wave cutoff energy of 700 eV was used for all calculations. Geometry relaxations were conducted using the Perdew-Burke-Ernzerhof version generalized gradient approximation (GGA-PBE) exchange-correlation functional<sup>25</sup> with a convergence criterion of 0.02 eV/Å for the force acting on each atom. A  $5 \times 5 \times 1$   $k$ -mesh was adopted. The electronic structures were evaluated by Heyd-Scuseria-Ernzerhof (HSE) hybrid functional<sup>27</sup> to overcome the bandgap underestimation in the semi-local exchange-correlation functional. The Hartree-Fock exchange factor is tested to be 27%, yielding the direct bandgap of 3.4 eV for wurtzite GaN bulk,<sup>28,29</sup> agreeing well with the experimental characteristics. Note that calculated bandgap for  $Al_2O_3$  and  $Sc_2O_3$  are 6.36 eV and 5.25 eV using this hybrid HF fraction, respectively, which are still 0.2 eV and 0.7 eV lower than that of the experimental values. The calculated total density of states (DOS) of the final relaxed bulk materials (structures shown in Fig. 1) are depicted in Fig. 2.

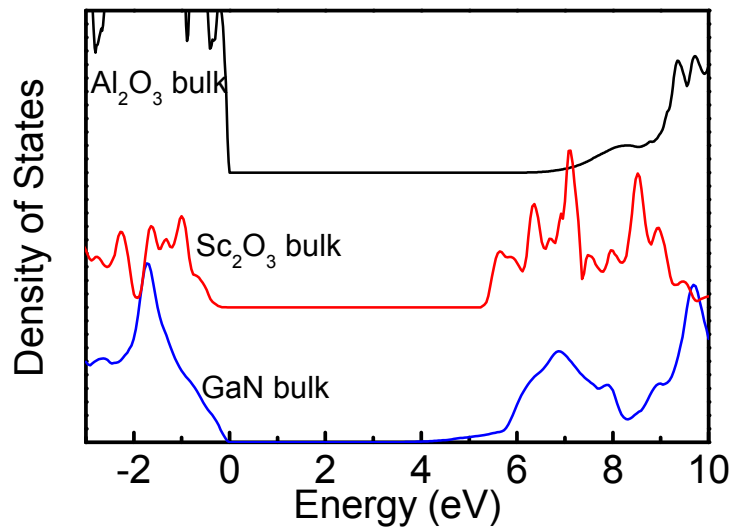


FIG. 2. Total density of states of bulk  $Al_2O_3$ ,  $Sc_2O_3$ , and GaN with hybrid functional calculation. Note that CBM of GaN bulk is too weak and the bandgap is obtained from the Gamma point data.

Although the deposited oxide normally adopts the amorphous phase, the essential requirement is the interface local bonding rather than long-range crystalline symmetry to meet the valence satisfaction.  $\text{Al}_2\text{O}_3$  possesses several symmetric phases, among which the most stable one is the hexagonal  $\alpha\text{-Al}_2\text{O}_3$  phase (i.e., corundum, or sapphire).<sup>30</sup> In the previous reports on  $\text{Al}_2\text{O}_3/\text{GaN}$ , the  $\alpha\text{-Al}_2\text{O}_3$  were adopted, benefiting from a smaller lattice mismatch with wurtzite GaN.<sup>20,21</sup> However the mass density ( $\sim 4.0 \text{ gm/cm}^3$ ) and bandgap ( $\sim 8.8 \text{ eV}$ ) in  $\alpha\text{-Al}_2\text{O}_3$  are too high compared to the amorphous one. Therefore, we adopted a modified  $\theta$ -phase  $\text{Al}_2\text{O}_3$  structure which has a mass density ( $\sim 3.5 \text{ g/cm}^3$ ), bandgap ( $\sim 6.6 \text{ eV}$ ) and atomic coordination close to the amorphous structure grown by ALD.<sup>30,31</sup> The  $\text{Al}_2\text{O}_3$  was strained to an orthorhombic structure and stretched laterally to achieve a good match with GaN (0001), before being fully relaxed to remove the stress. The atomic structure is shown in Fig. 1(b). For  $\text{Sc}_2\text{O}_3$ , the hexagonal phase was used (Fig. 1(c)), which matches GaN (0001) with a negligible lattice mismatch of only 3.7%. For the interface model, a thick vacuum (15 Å thickness) was added above oxide to avoid the image interaction due to the periodic boundary condition, and the bottom N dangling bonds (DBs) in GaN were passivated by pseudo-hydrogens. Half of the top O atoms were removed to generate an insulating oxide surface without gap states.

It is noted that to create a closed-shell structure, we built the interface supercell model of  $(2\times 4)$  in-plane periodicity, which contains an oxide surface slab and GaN (0001) slab with Ga-O bonding at the interface. The interface with Ga-O bonding is more stable than one with X-Ga or X-N interfacial bonding, because Ga is trivalent like Al to make sure the bonding characteristics of interfacial atoms is close to that in the bulk materials. Besides, Chokawa et al. has reported the Ga-Al interface shows much more interfacial defect states than the Ga-O model.<sup>21</sup> In this  $(2\times 4)$  interface, eight Ga and eight O atoms initially lie at the interface. For the covalent oxide  $\text{Al}_2\text{O}_3$ , the interfacial oxygen atoms perfectly saturate the Ga DBs. While for the ionic oxide  $\text{Sc}_2\text{O}_3$ , the structure is more complicated because both fourfold and sixfold O atoms exist in different layers within hexagonal  $\text{Sc}_2\text{O}_3$ . To gain the extra six electrons provided by eight Ga DBs, only four fourfold interfacial O atoms are required so that all the O DBs are occupied. Thus, we built the  $\text{Sc}_2\text{O}_3/\text{GaN}$  interface with only 50% interface O content (four fourfold interfacial O atoms) to satisfy the electron counting.

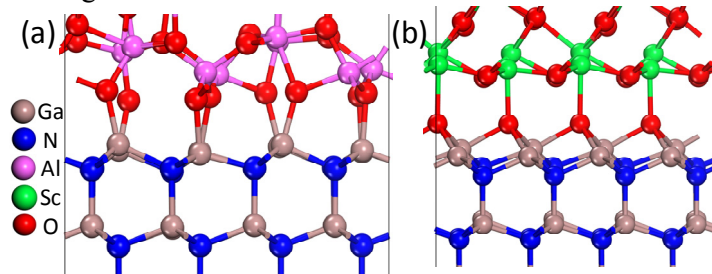


FIG. 3. The atomic structures of final relaxed (a)  $\text{Al}_2\text{O}_3/\text{GaN}$  and (b)  $\text{Sc}_2\text{O}_3/\text{GaN}$  interfaces. The species of atoms are indicated in the insert.

The lattice constant of relaxed GaN and  $\text{Sc}_2\text{O}_3$  bulk is 3.24 Å and 3.36 Å, respectively. Since the  $\text{Al}_2\text{O}_3$  structure was stretched laterally, it perfectly matches GaN (0001) surface. As shown in the final  $\text{Al}_2\text{O}_3/\text{GaN}$  interface structures in Fig. 3(a), the atomic structure in  $\text{Al}_2\text{O}_3$  side becomes different from that in the crystalline phase, but the local bonding and atomic coordinate remain the same. The interface is stable with a negligible roughness of only 0.3 Å at the interfacial Ga atom layer. The interfacial O atoms are either twofold or threefold, the same as its bulk bonding characteristics. Eight Ga-O bonds form at the interface and each Ga atom occupies one Ga-O bond. This perfectly saturates the Ga DBs and leads to an insulating interface. The average interfacial Ga-O bond length is 1.91 Å, indicating the stable covalent bonding characteristics. For the ionic oxide  $\text{Sc}_2\text{O}_3$  interface in Fig. 3(b), eight Ga atoms and four fourfold O atoms exist at the interface to satisfy the electron counting. These interfacial O species bond to one Sc atom on top and three Ga atoms underneath, the same as its bulk bonding characteristics. The interface roughness is 0.29 Å

with an average Ga-O bond length of 2.08 Å, close to that in the bulk  $\beta$ -Ga<sub>2</sub>O<sub>3</sub>. The interfacial interaction barely affects the local bonding of the Al (Sc) atoms and N atoms. All these results indicate an energy-stable X<sub>2</sub>O<sub>3</sub>/GaN configuration.

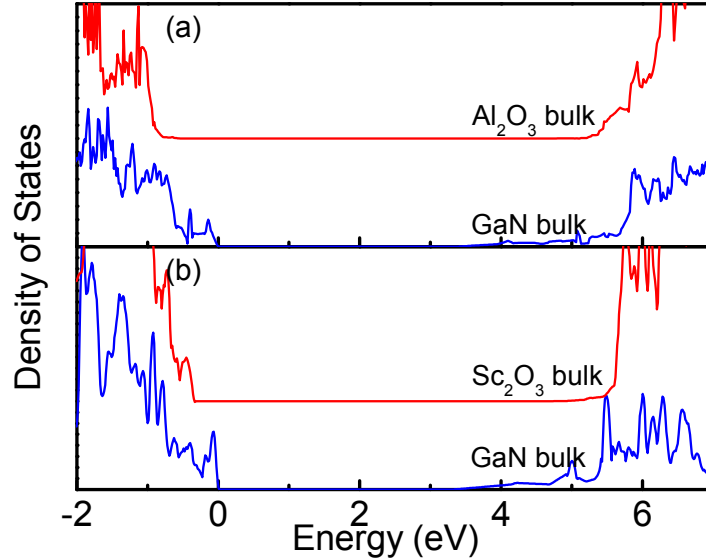


FIG. 4. Partial DOS of the bulk layer GaN and oxide atoms that are far away from the interface region in the (a) Al<sub>2</sub>O<sub>3</sub>/GaN and (b) Sc<sub>2</sub>O<sub>3</sub>/GaN model. VBM of GaN bulk is aligned to 0 eV.

The partial DOS of the bulk layer GaN and oxide atoms that are sufficiently distant away from the interface region in X<sub>2</sub>O<sub>3</sub>/GaN are presented in Fig. 4, where the valence band maximum (VBM) of GaN bulk is aligned to zero for convenience. It is pictorial that the prudently built models have an insulating interface with no gap states in the bandgap, owing to the perfect satisfaction of the electron-counting rule. Both interfaces feature the type-I band alignment with both the CBM and VBM at GaN side. This is consistent with the electron affinity as well as the experiment results. For power MOSFET application, GaN's CBM should be assuredly lower than that of oxide dielectric, otherwise, electrons could not be effectively confined in the semiconductor side and lead to large leakage current.

When oxide and semiconductor contact, discontinuous offsets (i.e., band offset) occur at both the valence band maximum (VBM) and conduction band minimum (CBM).<sup>12,13</sup> The band offset value can be roughly determined using the partial DOS scheme for the band edge line-up in the interface supercell model.<sup>32,33</sup> The energy difference between their valence band maxima (i.e., VBO) is roughly observed to be 0.9 eV and 0.4 eV for Al<sub>2</sub>O<sub>3</sub>/GaN and Sc<sub>2</sub>O<sub>3</sub>/GaN in Fig. 4, respectively. Their counterpart CBOs are derived by using the calculated values of the band gaps of GaN (3.4 eV) and X<sub>2</sub>O<sub>3</sub> (6.36 eV and 5.25 eV). In this work, we focus on another more accurate scheme to determine the band alignment using the core-level state,<sup>22</sup> for the assumption that the energy difference between the valence band maximum and the core-level state maintains a constant value even under different environment. We used the Ga-3*d* and O-2*s* core-level state in the bulk-like region which are unaffected by the interface effect for reference, and derived the VBM of the individual side in the interface model with respect to this, and thus the VBO as the difference.

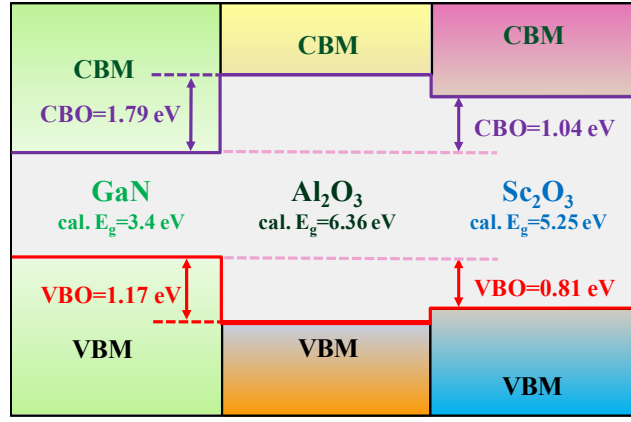


FIG. 5. Schematic band alignment diagram of  $\text{Al}_2\text{O}_3/\text{GaN}$  and  $\text{Sc}_2\text{O}_3/\text{GaN}$  interfaces using the core-level alignment. The valence band offset is determined using the core-level alignment method, which provides more accurate results. The CBO is defined as the difference between the calculated bandgap and VBO values.

The schematic band alignment diagram of  $\text{X}_2\text{O}_3/\text{GaN}$  interface using the core-level alignment is shown in Fig. 5. It is worth noting that the calculated bandgap for  $\text{Al}_2\text{O}_3$  and  $\text{Sc}_2\text{O}_3$  are 6.36 eV and 5.25 eV, respectively, which are still 0.2 eV and 0.7 eV lower than that of the experimental data.<sup>6,15</sup> The results presented here can still be appreciated for the experimental bandgap value of GaN ( $E_g=3.4$  eV) is well reproduced. The calculated VBO is 1.17 eV for  $\text{Al}_2\text{O}_3/\text{GaN}$  and 0.81 eV for  $\text{Sc}_2\text{O}_3/\text{GaN}$  interface, respectively. Taking advantage of the calculated oxide bandgap, the corresponding CBO is set to be 1.79 eV and 1.04 eV, respectively.

TABLE I: Band alignment comparison between our calculated  $\text{X}_2\text{O}_3/\text{GaN}$  interface values and the experimental reports. Note that the bandgap and BOs described in this work are all derived by *hybrid functional calculations*.

$E_g$ of $\text{Al}_2\text{O}_3$ (eV)	$E_g$ of GaN (eV)	VBO (eV)	CBO (eV)	Data
6.36	3.4	1.17	1.79	This work
6.7	3.4	2.1	1.2	Ref. [6]
6.5	3.4	1.8	1.3	Ref. [7]
6.6	3.4	1.0	2.2	Ref. [8]
-	-	0.7	-	Ref. [9]
6.4	3.4	0.05	2.95	Ref. [14]
$E_g$ of $\text{Sc}_2\text{O}_3$ (eV)	$E_g$ of GaN (eV)	VBO (eV)	CBO (eV)	Data
5.25	3.40	0.81	1.04	This work
6.0	3.44	0.42	2.14	Ref. [15]
6.3	3.42	0.84	2.04	Ref. [16]

It is meaningful to compare the calculated band alignment with the experimental values. All the experimental reported band offsets between  $\text{Al}_2\text{O}_3/\text{GaN}$  and  $\text{Sc}_2\text{O}_3/\text{GaN}$  are listed in Table I, with the calculated data (this work) for reference. It can be seen that the calculated VBOs all fall within the experiment range. At variance with the experimental derived CBOs, the calculated CBOs are lower than several references. It is because the oxide bandgap is still underestimated (0.2 eV and 0.7 eV lower than that of the experimental data, respectively<sup>6,15</sup>). If taking advantage of the experimental bandgap ( $\sim 6.6$  eV for  $\text{Al}_2\text{O}_3$  and  $\sim 6.0$  for  $\text{Sc}_2\text{O}_3$ <sup>6,15</sup>) and our calculated VBOs, the newly derived CBO will be  $\sim 2.0$  eV for  $\text{Al}_2\text{O}_3$  interface and  $\sim 1.8$  for  $\text{Sc}_2\text{O}_3$  interface, which agrees better with the experimental conduction band offset values. Notably, the CBM at GaN side is  $\sim 2.0$

eV lower than that of  $X_2O_3$  in both interface, well satisfying the 1 eV criterion for confining electrons at semiconductor side.<sup>12</sup> In GaN-based power device applications, the gate electrode could suffer a large gate voltage to drive the power module. With the  $\sim 2.0$  eV CBOs the electrons can be effectively confined in the GaN side, further confirming that both  $Al_2O_3$  and  $Sc_2O_3$  are ideal dielectric materials for GaN-based MOSFET device applications.

In conclusion, the interfacial bonding, electronic structures and band offset of  $Al_2O_3/GaN$  and  $Sc_2O_3/GaN$  interface were intensively investigated. By prudently modeling based on electron counting rule, the insulating interface model with small interfacial roughness and clean bandgap was obtained. The valence band offset is derived to be  $\sim 1.2$  and  $\sim 0.8$  eV, respectively, well coinciding with the experiment results. The large conduction band offset ( $\sim 2.0$  eV) is sufficient for effectively confining electrons in GaN-based MOSFET device with  $Al_2O_3$  or  $Sc_2O_3$  as gate dielectric.

The authors acknowledge funding from EPSRC Grant No. EP/P005152/1.

- <sup>1</sup> J. Y. Tsao, S. Chowdhury, M. A. Hollis, D. Jena, N. M. Johnson, K. A. Jones, R. J. Kaplar, S. Rajan, C. G. Van de Walle, E. Bellotti, C. L. Chua, R. Collazo, M. E. Coltrin, J. A. Cooper, K. R. Evans, S. Graham, T. A. Grotjohn, E. R. Heller, M. Higashiwaki, M. S. Islam, P. W. Juodawlkis, M. A. Khan, A. D. Koehler, J. H. Leach, U. K. Mishra, R. J. Nemanich, R. C. N. Pilawa-Podgurski, J. B. Shealy, Z. Sitar, M. J. Tadjer, A. F. Witulski, M. Wraback, and J. A. Simmons, *Adv. Electron. Mater* **4**, 1600501 (2018).
- <sup>2</sup> K. J. Chen, O. Häberlen, A. Lidow, C. L. Tsai, T. Ueda, Y. Uemoto, and Y. Wu, *IEEE Trans. Electron Devices* **64**, 779 (2017).
- <sup>3</sup> R. Vetry, N. Q. Zhang, S. Keller, and U. K. Mishra, *IEEE Trans. Electron Device* **48**, 560 (2001).
- <sup>4</sup> R. Mehandru, B. Luo, J. Kim, F. Ren, B. P. Gila, A. H. Onstine, C. R. Abernathy, S. J. Pearton, D. Gotthold, R. Birkhahn, B. Peres, R. Fitch, J. Gillespie, T. Jenkins, J. Sewell, D. Via, and A. Crespo, *Appl. Phys. Lett.* **82**, 2530 (2003).
- <sup>5</sup> X. Wang, O. I. Saadat, B. Xi, X. Lou, R. J. Molnar, T. Palacios, and R. G. Gordon, *Appl. Phys. Lett.* **101**, 232109 (2012).
- <sup>6</sup> J. Yang, B. S. Eller and R. J. Nemanich, *J. Appl. Phys.* **116**, 123702 (2014).
- <sup>7</sup> J. Yang, B. S. Eller, C. Zhu, C. England, and R. J. Nemanich, *J. Appl. Phys.* **112**, 53710 (2012).
- <sup>8</sup> Y. Jia, J. S. Wallace, E. Echeverria, J. A. Gardella, and U. Singiseti, *Phys. Status Solidi B* **254**, 1600681 (2017).
- <sup>9</sup> T. L. Duan, J. S. Pan and D. S. Ang, *Appl. Phys. Lett.* **102**, 201604 (2013).
- <sup>10</sup> S. Yang, Z. Tang, K. Wong, Y. Lin, C. Liu, Y. Lu, S. Huang, and K. J. Chen, *IEEE Electron Device Lett.* **34**, 1497 (2013).
- <sup>11</sup> D. M. Zhernokletov, M. A. Negara, R. D. Long, S. Aloni, D. Nordlund, and P. C. McIntyre, *ACS Appl. Mater. Interfaces* **7**, 12774 (2015).
- <sup>12</sup> J. Robertson, *J. Vac. Sci. Technol. B* **18**, 1785 (2000).
- <sup>13</sup> Y. Guo, H. Li, S. J. Clark, and J. Robertson, *J. Phys. Chem. C* **123**, 5562 (2019).
- <sup>14</sup> M. R. Coan, J. H. Woo, D. Johnson, I. R. Gatabi, and H. R. Harris, *J. Appl. Phys.* **112**, 24508 (2012).
- <sup>15</sup> J. J. Chen, B. P. Gila, M. Hlad, A. Gerger, F. Ren, C. R. Abernathy, and S. J. Pearton, *Appl. Phys. Lett.* **88**, 142115 (2006).
- <sup>16</sup> C. Liu, E. F. Chor, L. S. Tan, and Y. Dong, *Phys. Status Solidi C* **4**, 2330 (2007).
- <sup>17</sup> M. D. Pashley, *Phys. Rev. B* **40**, 10481 (1989).
- <sup>18</sup> L. Lin and J. Robertson, *Appl. Phys. Lett.* **98**, 82903 (2011).
- <sup>19</sup> L. Lin, Y. Guo, R. Gillen, and J. Robertson, *J. Appl. Phys.* **113**, 134103 (2013).
- <sup>20</sup> M. B. Pereira, E. M. Diniz and S. Guerini, *Adv. Cond. Matter Phys.* **2015**, 1 (2015).
- <sup>21</sup> K. Chokawa, E. Kojima, M. Araidai, and K. Shiraishi, *Phys. Status Solidi B* **255**, 1700323 (2018).
- <sup>22</sup> E. A. Kraut, R. W. Grant, J. R. Waldrop, and S. P. Kowalczyk, *Phys. Rev. Lett.* **44**, 1620 (1980).
- <sup>23</sup> S. J. Clark, M. D. Segall, C. J. Pickard, P. J. Hasnip, M. I. J. Probert, K. Refson, and M. C. Payne, *Z. Kristallogr.* **220**, 567 (2005).
- <sup>24</sup> S. J. Clark and J. Robertson, *Physical Review B* **82**, 85208 (2010).
- <sup>25</sup> J. P. Perdew, K. Burke and M. Ernzerhof, *Phys. Rev. Lett.* **77**, 3865 (1996).
- <sup>26</sup> J. Heyd, G. E. Scuseria and M. Ernzerhof, *J. Chem. Phys.* **124**, 219906 (2006).
- <sup>27</sup> Z. Zhang, B. Li, Q. Qian, X. Tang, M. Hua, B. Huang, and K. J. Chen, *IEEE Trans. Electron Devices* **64**, 4036 (2017).
- <sup>28</sup> Z. Zhang, Q. Qian, B. Li, and K. J. Chen, *ACS Appl. Mater. Interfaces* **10**, 17419 (2018).
- <sup>29</sup> D. Liu, S. J. Clark and J. Robertson, *Appl. Phys. Lett.* **96**, 32905 (2010).
- <sup>30</sup> D. Liu and J. Robertson, *Microelectron. Eng.* **86**, 1668 (2009).
- <sup>31</sup> L. Lin, K. Xiong and J. Robertson, *Appl. Phys. Lett.* **97**, 242902 (2010).

<sup>32</sup>Z. Zhang, R. Cao, C. Wang, H. Li, H. Dong, W. Wang, F. Lu, Y. Cheng, X. Xie, H. Liu, K. Cho, R. Wallace, and W. Wang, *ACS Appl. Mater. Interfaces* **7**, 5141 (2015).